



Experimental realization of dual task processing with a photonic reservoir computer

Jeremy Vatin, Damien Rontani, Marc Sciamanna

► To cite this version:

Jeremy Vatin, Damien Rontani, Marc Sciamanna. Experimental realization of dual task processing with a photonic reservoir computer. APL Photonics, 2020, 5 (8), pp.086105. 10.1063/5.0017574 . hal-02919602

HAL Id: hal-02919602

<https://hal.science/hal-02919602>

Submitted on 23 Aug 2020

HAL is a multi-disciplinary open access archive for the deposit and dissemination of scientific research documents, whether they are published or not. The documents may come from teaching and research institutions in France or abroad, or from public or private research centers.

L'archive ouverte pluridisciplinaire **HAL**, est destinée au dépôt et à la diffusion de documents scientifiques de niveau recherche, publiés ou non, émanant des établissements d'enseignement et de recherche français ou étrangers, des laboratoires publics ou privés.

Experimental realization of dual task processing with a photonic reservoir computer

Cite as: APL Photonics 5, 086105 (2020); <https://doi.org/10.1063/5.0017574>

Submitted: 22 April 2020 . Accepted: 28 July 2020 . Published Online: 13 August 2020

Jeremy Vatin , Damien Rontani, and Marc Sciamanna 



View Online



Export Citation



CrossMark

ARTICLES YOU MAY BE INTERESTED IN

Photonic neuromorphic information processing and reservoir computing


APL Photonics 5, 020901 (2020); <https://doi.org/10.1063/1.5129762>

Ultra-sensitive refractive index gas sensor with functionalized silicon nitride photonic circuits


APL Photonics 5, 081301 (2020); <https://doi.org/10.1063/5.0013577>

Optical parametric gain in CMOS-compatible sub-100 μm photonic crystal waveguides

APL Photonics 5, 066108 (2020); <https://doi.org/10.1063/5.0003633>



THE ADVANCED MATERIALS MANUFACTURER®



additive manufacturing epitaxial crystal growth cerium oxide polishing powder silver nanoparticles sputtering targets III-IV semiconductors CVD precursors europium phosphors

deposition slugs OLED Lighting spintronics solar energy osmium nanoribbons thin films chalcogenides AuNPs GDC Li-ion battery electrolytes 99.999% ruthenium spheres

endohedral fullerenes copper nanoparticles diamond micropowder CIGS MBE grade materials palladium catalysts flexible electronics beta-barium borate borosilicate glass dysprosium pellets YBCO pyrolytic graphite 3d graphene foam indium tin oxide mesoporous silica raman substrates sapphire windows tungsten carbide InGaAs barium fluoride carbon nanotubes lithium niobate scandium powder

gallium lump glassy carbon nanodispersions InAs wafers laser crystals ultra high purity materials MOFs surface functionalized nanoparticles organometallics quantum dot rare earth metals photovoltaics refractory metals MOCVD superconductors transparent ceramics ultra high purity silicon

Now Invent.™
The Next Generation of Material Science Catalogs

American Elements opens up a world of possibilities so you can **Now Invent!**

Over 15,000 certified high purity laboratory chemicals, metals, & advanced materials and a state-of-the-art Research Center. Printable GHS-compliant Safety Data Sheets. Thousands of new products. And much more. All on a secure multi-language "Mobile Responsive" platform.

perovskite crystals yttrium iron garnet alternative energy h-BN gold nanocubes graphene oxide macromolecules photonics rhodium sponge fiber optics beamsplitters infrared dyes zeolites fused quartz metallocenes platinum ink buckyballs Ti-6Al-4V

www.americanelements.com

Experimental realization of dual task processing with a photonic reservoir computer

Cite as: APL Photon. 5, 086105 (2020); doi: 10.1063/5.0017574

Submitted: 22 April 2020 • Accepted: 28 July 2020 •

Published Online: 13 August 2020



Jeremy Vatin,^{a)}  Damien Rontani, and Marc Sciamanna 

AFFILIATIONS

Chair in Photonics, LMOPS EA 4423 Laboratory, CentraleSupélec and Université Lorraine, 2 rue Edouard Belin, F-57070 Metz, France

^{a)} Author to whom correspondence should be addressed: jeremy.vatin@centralesupelec.fr

ABSTRACT

We experimentally demonstrate the possibility to process two tasks in parallel with a photonic reservoir computer based on a vertical-cavity surface-emitting laser (VCSEL) as a physical node with time-delay optical feedback. The two tasks are injected optically by exploiting the polarization dynamics of the VCSEL. We test our reservoir with the very demanding task of nonlinear optical channel equalization as an illustration of the performance of the system and show the recover of two signals simultaneously with an error rate of 0.3% (3%) for a 25 km-fiber distortion (50 km-fiber distortion) at a processing speed of 51.3 Mb/s.

© 2020 Author(s). All article content, except where otherwise noted, is licensed under a Creative Commons Attribution (CC BY) license (<http://creativecommons.org/licenses/by/4.0/>). <https://doi.org/10.1063/5.0017574>

I. INTRODUCTION

Building energy efficient systems to process data currently performed by computer is one of the focus problems that photonic reservoir computing is trying to address. A reservoir computing system is a specific kind of neural network with a recurrent topology, i.e., coupling signals and information are not propagating unidirectional in the network structure. The training, consisting of adjusting the interconnection weight between the neurons for this particular structure, is usually difficult and data intensive as it scales with the square of the network size to solve a specific task. This also implies that the physical architecture with many tunable degrees of freedom should be designed, which represents a significant technical challenge for the development of efficient hardware platforms. A reservoir computing system overcomes these hurdles by not realizing the training through internal weight adjustments but by keeping it fixed and training a readout layer unidirectionally connected to the recurrent network. This can be achieved with a simple linear regression at the readout with simple regression algorithms.^{1,2} This is specifically interesting as it allows the use of physical components for a hardware implementation of a neural network. Several architectures using this specific principle already exist.^{3–7}

However, realizing a large physical neural network remains a technical challenge especially with photonic devices. Hence, a

solution was proposed with time-delay reservoir computing: Instead of using physical neurons, only one physical neuron is used, and several virtual neurons are temporally spread along a delay line.⁸ The time separation between virtual neurons is set to be smaller than the physical-neuron response time so that the neurons remain in a sustained transient dynamics, which effectively translates into time-multiplexed interconnection between the virtual neurons. In that framework, adding neurons only requires lengthening the delay line. Several photonic architectures use this specific technique, with either an optoelectronic^{4,9,10} or an all-optical^{11–17} delay line.

The vertical-cavity surface-emitting laser (VCSEL) is a good candidate to realize a time-delay reservoir computer and process data in optical networks as it is widely used in optical telecommunication networks. One of VCSEL's specificity is light emission along two orthogonal linear polarization modes and a faster modulation frequency than an edge-emitting laser.¹⁸ We have already proven numerically¹⁹ and experimentally²⁰ that a VCSEL-based time-delay reservoir computer is able to efficiently perform computation tasks, with state-of-the-art performance on various tasks such as chaotic time-series prediction and nonlinear WIFI channel equalization.

Parallel processing of two tasks was originally proposed in Ref. 13 using single-mode dynamics of a laser diode. Using the

multimode polarization dynamics of a laser diode has also been considered to perform simultaneously several tasks. It has been shown theoretically that using two longitudinal modes of an edge-emitting laser,¹⁷ the two modes of a semiconductor ring laser¹⁵ or the two polarization modes of a VCSEL²¹ enable parallel processing with a time-delay reservoir computing architecture. We thus experimentally address here the question of whether a VCSEL-based photonic reservoir, which exhibits two polarization modes, is able to perform efficiently two tasks consisting of the recovery of two optical signals being distorted by a fiber.

In this article, we present an experimental realization of a reservoir computer processing two tasks simultaneously. This reservoir computer is based on the time-delay reservoir architecture, using a VCSEL as a physical node. The two tasks are injected optically in each polarization mode of the VCSEL. By carefully choosing the operating point of the reservoir computer, we show the possibility to tune the performance of the system on each processed task. As an illustration, we test our reservoir on the nonlinear optical channel equalization. This task is very demanding as signals sent in optical fiber are distorted due to several nonlinear effects, such as chromatic dispersion and Kerr effect.²² More specifically, we are able to recover

two signals simultaneously distorted by 25 km and by 50 km of fiber and sent at 25 Gb/s with a mean error rate of 0.3% at 25 km and of 3% at 50 km, at a processing speed of 51.3 Mb/s.

II. METHOD

The experimental setup is depicted in Fig. 1. The reservoir itself is the same as the one we have previously studied in Ref. 20: It comprises a VCSEL (Raycan) as a physical node, which emits light at 1552.75 nm for the dominant linear polarization mode (LP_x) and at 1552.89 nm for the depressed polarization mode (LP_y). The bias current of the VCSEL is set at 4.5 mA, which corresponds to 1.5 times the threshold current. This choice of pumping current is based on the previous numerical analysis we conducted in Ref. 19, showing that a pumping current close to the current threshold lead to high-memory capacity and overall computing performance for the time-delay VCSEL-based reservoir computer. The feedback loop is made of a SMF-28 single mode fiber (standard telecommunication fiber) resulting in a delay line of $\tau = 39.4$ ns. As only one calculation step can be performed per round-trip, this length imposes to a

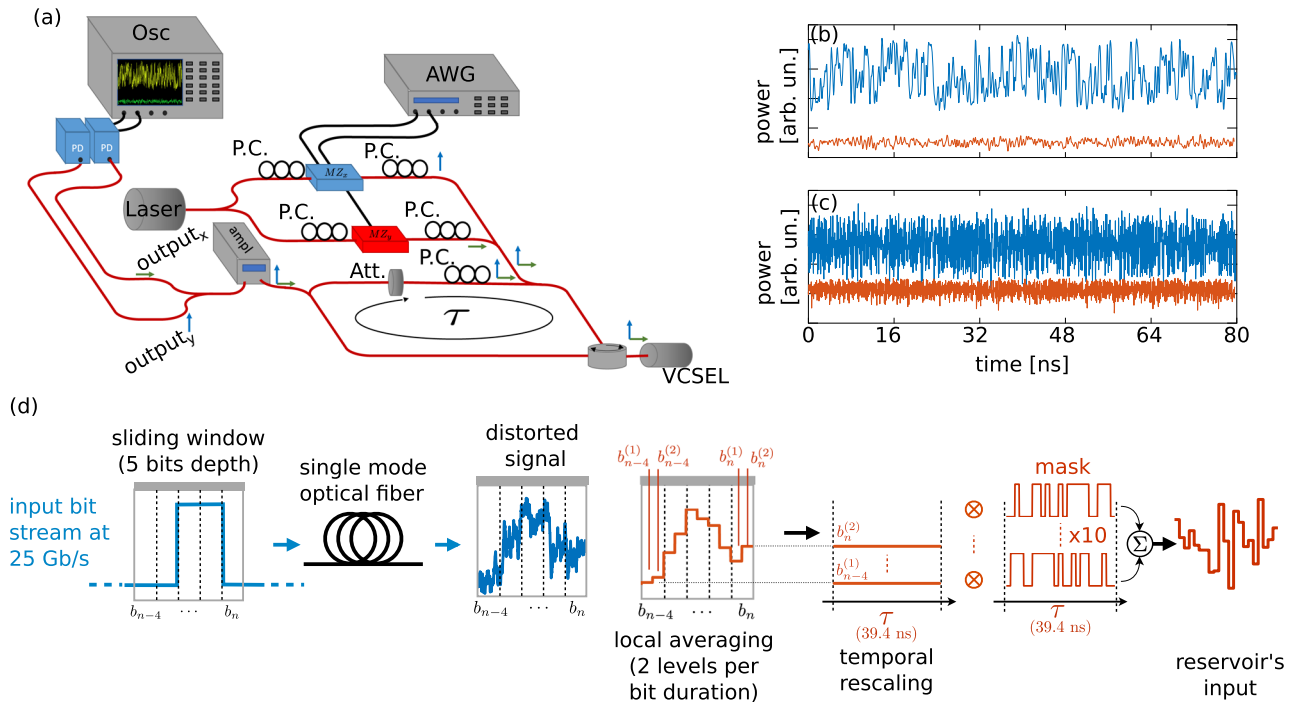


FIG. 1. (a) Scheme of the experiment. The two masked signals are sent on the two modulators. Each input signal is aligned with a different polarization mode of the VCSEL. MZ: Mach-Zehnder modulator, P.C.: polarization controller, AWG: arbitrary waveform generator, Att: attenuator, Osc: Oscilloscope, ampl: amplifier, and PD: photodiode. (b) Example of two input streams generated by the AWG. The blue line corresponds to the input stream injected in the dominant polarization mode (LP_x), and the red line corresponds to the stream injected in the depressed polarization mode (LP_y) of the VCSEL. (c) example of signals recorded at the output of the reservoir computing system. The blue line corresponds to the response of the dominant polarization mode (LP_x), and the red line corresponds to the response of the depressed polarization mode (LP_y) of the VCSEL. (d) Scheme of the preprocessing method. The signal at the output of the fiber is averaged at twice the frequency of the input data stream, giving symbols $b_n^{(1)}$ and $b_n^{(2)}$ for each bit b_n . This signal is temporally rescaled so that each symbol duration is τ . The ten values $b_{n-4}^{(1)}$, $b_{n-4}^{(2)}$, to $b_n^{(1)}$ and $b_n^{(2)}$ are masked with a mask of $10 \times N$ values and used as an input of the reservoir to reconstruct b_{n-2} .

processing speed of 25.65 MHz per task, thus 51.3 MHz for two tasks. The speed of the system could be increased by reducing the length of the delay line, which was not possible in our case. To optimize our use of the VCSEL dynamics, we set the inter-nodes delay $\theta = 0.04$ ns according to previous simulations¹⁹ and the frequency limitation of the experimental components (i.e., oscilloscope, arbitrary waveform generator and modulators): The optimal delay between virtual nodes that exploits the best VCSEL's transient response is $\theta^* = 0.02$ ns; however, the modulation bandwidth of our arbitrary waveform generator (AWG) is at 25 GHz. We use for the training and testing of the reservoir only one every two nodes separated by $2\theta = 0.08$ ns due to the memory limitation of the computer performing the training, thus leading to consider $N = 492$ nodes instead of $N = 984$. Considering an increasing number of virtual nodes while keeping the feedback delay fixed, we observed numerically an improvement of the performance up to $N_{th} = 100$. Beyond this threshold value, increasing the size of the virtual network will only lead to marginal improvement in the RC performance. In our experience, we choose $N = 492 > N_{th}$ for experimental convenience rather than using all the accessible virtual nodes to speed up the training phase without compromising on the performance. There is also a polarization controller (P.C.) to control the optical polarization along the feedback loop. Finally, an optical attenuator Keysight 81577A (Att.) is used to control the feedback strength. In this article, the results presented are obtained with the isotropic feedback configuration, i.e., the orientation of the two VCSEL's polarization modes ($LP_{x,y}$) are preserved in the external cavity prior to being fed back. Accordingly to the results obtained in Ref. 19, there is an optimum operating point for each value of the feedback strength while varying the injection power. This is why we set the feedback attenuation η to 17 dB to guarantee that enough power is injected to find this best operating point.

The input layer is primarily composed of an arbitrary waveform generator (AWG) AWG700002A from Tektronix, a tunable laser Tunics T100S from Yanista, and two Mach-Zehnder modulators ($MZ_{x,y}$) with a bandwidth of 12.5 GHz. Both modulators are working in their linear regime. The light emitted by the tunable laser is split in two different beams and sent in the two different modulators. The wavelength of this laser is set to 1552.82 nm so that its wavelength is equally separated from the frequencies of the main and depressed polarization modes of the VCSEL, as presented in Fig. 2. By doing so, we ensure that having the same power in both linear polarization modes at the output of the modulators, the power is equally distributed among the two linear polarization modes of the injected VCSEL. Shifting the frequency of the master laser to one of the polarization modes of the VCSEL leads to a more efficient optical injection in this mode and therefore enhances the response of this mode at the expense of the response of the other mode, for which the optical injection is reduced. The two different masked input streams, corresponding to the two tasks $T_{x,y}$ to be processed, are used to drive both modulators and are generated by the AWG at a symbol rate of 25 GS/s for each stream. The output power of the modulator is controlled by an optical attenuator built inside each modulator. This allows the independent change of the injected power $P_{inj,x,y}$ of the tasks $T_{x,y}$. At the modulators output, the optical polarization of the input stream containing T_x is aligned with the main polarization mode (LP_x) of the VCSEL and the one of the input stream containing T_y with the depressed polarization mode (LP_y). An example of

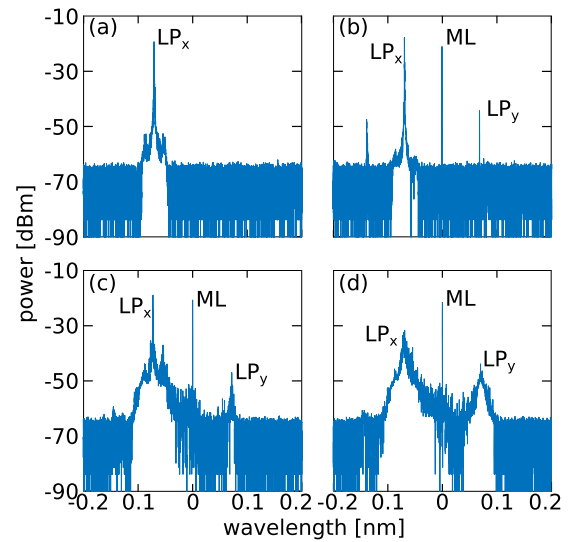


FIG. 2. Optical spectra of the system under different operation conditions. LP_x : dominant polarization mode, LP_y : depressed polarization mode, and ML: master laser. (a) VCSEL with isotropic feedback, $\eta = 17$ dB. (b) Reservoir computer with optical injection on both polarization modes without modulation, $P_{inj,x} = P_{inj,y} = 0.08$ mW, $\eta = 17$ dB, (c) reservoir computer with optical injection on both polarization modes with modulation, $P_{inj,x} = P_{inj,y} = 0.08$ mW, $\eta = 17$ dB, and (d) reservoir computer with optical injection on both polarization modes with modulation, $P_{inj,x} = 0.08$ mW, $P_{inj,y} = 0.4$ mW $\eta = 17$ dB.

input streams is given in Fig. 1(b). Both beams are then recombined and sent in the reservoir computer.

The response of the reservoir is recorded at the output layer: The signal is first amplified with an erbium-doped fiber amplifier (EDFA) from Lumibird. Then, the two polarization modes of the VCSEL are separated and recorded with two photodiodes Newport 1544-B 12 GHz bandwidth, connected to an oscilloscope Tektronix DPO 71604C 16 GHz bandwidth with two channels at 50 GS/s. Examples of the experimental time series recorded for each polarization mode of the VCSEL are given in Fig. 1(c). The signal-to-noise ratio (SNR) has been experimentally measured at 21 dB.

With the high-resolution optical spectrum analyzer BOSA from Aragon Photonics, we can study the spectral dynamics of the system in different configurations. Figure 2(a) shows the experimental optical spectrum of the reservoir computer without injection and with optical feedback. The VCSEL is lasing at 1552.72 nm, the wavelength of its dominant polarization mode. The dominant mode LP_x of the VCSEL has a spectral width of 5.72 GHz with an attenuation of 17 dB in the feedback loop. The two smaller side peaks are induced by the undamped relaxation oscillations of the VCSEL,²³ which frequency is measured at 3.73 GHz. Figure 2(b) presents the spectrum of the reservoir with injection but without modulating input: Under this condition, the VCSEL is emitting light only in its dominant polarization mode, with the wavelength of the master laser at 1552.82 nm. We notice that the slave laser exhibits wave-mixing dynamics and that it is not locked to the master laser. When modulating the master laser, its spectrum broadens and overlaps the two wavelengths of the VCSEL, as shown in Figs. 2(c) and 2(d). This allows the VCSEL

to react to the master laser and to respond according to the modulated input. This response also broadens the spectra of the two polarization modes of the VCSEL. The spectral width of the dominant polarization mode LP_x detuned from the modulated input by 9.45 GHz. We observe also that injecting more power in the depressed mode LP_y forces its emission despite not lasing when the VCSEL is free-running.

We have tested the dual-tasking performance of our reservoir at solving a nonlinear optical channel equalization, which aims at reconstructing a transmitted signal only from the given distorted signal at the channel's output. We have chosen a single-mode optical fiber for the telecommunication channel. The distortion introduced by this channel is simulated using the nonlinear Schrödinger equation, which models the propagation of a signal in the fiber. This equation reads as²⁴

$$i \frac{\partial E(z, t)}{\partial z} = -i \frac{\alpha}{2} E(z, t) + \frac{\beta_2}{2} \frac{\partial^2 E(z, t)}{\partial t^2} - \gamma |E(z, t)|^2 E(z, t), \quad (1)$$

where $E(z, t)$ is the slowly varying envelop of the optical field, α is the attenuation of the fiber, β_2 is the second order coefficient of dispersion, and γ refers to the nonlinearity of the fiber. We have chosen the coefficient of the SMF-28 fiber, which is the single mode silica fiber used for long haul transmission, with $\alpha = 0.2 \text{ dB km}^{-1}$, $\beta_2 = -21.4 \text{ ps}^2 \text{ km}^{-1}$, and $\gamma = 1.2 \text{ W}^{-1} \text{ km}^{-1}$ (Ref. 25). We used the split-step Fourier method to numerically integrate the equation. The signal we use as an input of the fiber is a series of bits using pulse amplitude modulation (PAM) at 25 Gb/s. The power of the input pulse is set to 4 mW. This value is small enough to avoid significant distortion induced by the Kerr nonlinearity of the optical fiber. To compare our results with the state-of-the-art achieved with time-delay photonic reservoir computer, we perform the recovery after a 25 km and a 50 km long optical fiber.^{16,26} Examples of input signals are presented in Figs. 4(a) and 5(a), and their respective distorted versions after propagating in the optical fiber 25 km and 50 km are given in Figs. 4(b) and 5(b), respectively. The distortion induced by 25 km of optical fiber still allows us to identify the long lasting pulse. However, after 50 km, the distortion is more pronounced and does not allow straightforward retrieval of any section of the original signal.

The signal at the output of the simulated channel is a time continuous signal. Similar to the method used by Argyris *et al.* in Ref. 26, for each bit, we associate two features values $b_n^{(1)}$ and $b_n^{(2)}$, which are the time-average values of the upper half and the lower half of the distorted signal for the duration of one bit. The input of the reservoir is realized by masking each feature value for five consecutive bits, hence using 10 different masks (one per input value) of 985 values, which are then summed together. The masked input of the reservoir $J_{n-2}(t)$ at the step $n - 2$ reads

$$J_{n-2}(t) = \sum_{i=0}^4 b_{n-i}^{(1)} \times M_{2i}(t) + \sum_{i=0}^4 b_{n-i}^{(2)} \times M_{2i+1}(t), \quad (2)$$

where $M_i(t)$ is one of the ten different masks. A graphical illustration of the preprocessing is given in Fig. 1(d). At the output of the reservoir, we train the system by linear regression with $N = 492$ nodes to recover bits b_{n-2} . For each node, we use as a state the values of the optical power of the two orthogonal polarization modes (LP_x and

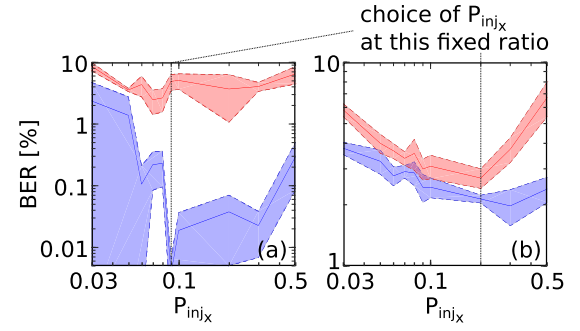


FIG. 3. Performance on the nonlinear channel equalization task as a function of the injection power in the main polarization mode P_{inj_x} for a fixed ratio of injection power $\frac{P_{inj_y}}{P_{inj_x}}$ at 0.3. (a) Performance of the recovery of a distortion due to 25 km of optical fiber. (b) Performance of the recovery of a distortion due to 50 km of optical fiber. The blue curve corresponds to the performance of the task T_x , and the red one corresponds to the performance of the task T_y . The dotted line corresponds to the choice of P_{inj_x} reported in Figs. 4 and 5 for this specific case.

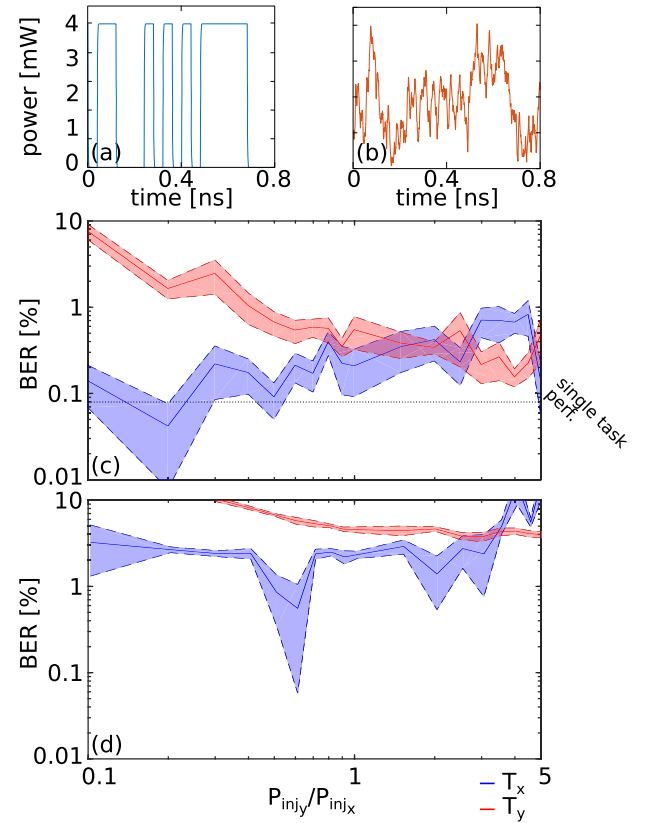


FIG. 4. Performance on the nonlinear channel equalization task after propagating 25 km in a communication channel made of optical fiber as a function of the ratio of injection P_{inj_y}/P_{inj_x} . (a) Example of the signal sent at the input of the fiber. (b) Corresponding received signal after 25 km of fiber. The blue curves corresponds to the performance of the task T_x , and the red curves corresponds to the performance of the task T_y for (c) the reservoir computer and (d) the linear classifier. The lighter area shows the standard deviation of the performance. The dotted line shows the performance of the reservoir performing the single task.

LP_y). Two different linear regressions are performed, one for each task T_x and T_y , using the whole state of the reservoir. The equations of the regressions are $S \times \omega_x = b_{T_x}$ and $S \times \omega_y = b_{T_y}$, where S is the reservoir's state matrix containing the power associated with the dominant (LP_x) and depressed (LP_y) polarization mode. ω_i is the vector containing the readout layer weights obtained from linear regression, and b_{T_i} is the vector containing the target output of the task T_i . Exploiting the two LP modes for each regression stems from nonlinear mixing the two input data streams in the VCSEL dynamics so that the two polarization modes contains part of the information of both processed tasks. For the training of the reservoir, we use 20 000 samples, i.e., sliding block of five consecutive distorted bits. Since we record optical power of $LP_{x,y}$ modes for the 492 nodes, the size of S is $20\,000 \times 984$. The performance of the reservoir is tested on 5380 samples and measured using the bit error rate (BER).

As already stated, for each value of the feedback strength, there is a corresponding optimal injection power for the reservoir computer.¹⁹ That is why we vary only the injected power, while keeping

the value of the feedback strength fixed. This allows reducing the dimension of the space parameters to explore to find the best experimental operating point. By finding the best operating point, we ensure for our VCSEL-based reservoir computing system to have a combination of large memory capacity (i.e., long fading memory) and large computational ability (i.e., good aptitude for approximation and generalization), as demonstrated in our previous numerical analysis.¹⁹ Furthermore, we aim at showing the tunable parameters that can control the performance of the two processed tasks T_x and T_y . Figures 4 and 5 present the influence of the ratio of injection power $\frac{P_{inj_y}}{P_{inj_x}}$ on the performance of the two processed tasks. To produce these figures, we first find the best operating point for each value of this ratio: We sweep the value of P_{inj_x} (an example is provided in Fig. 3), and P_{inj_y} is then fixed by the value of the ratio. As a result, we find the value of P_{inj_x} that minimizes the mean BER for both T_x and T_y . This optimal value is then reported in the graph (this is why Figs. 4 and 5 do not contain any information on the effective injected power). Figure 3 shows an example of the method used to produce the performance figures.

We first present the influence of the injected power on the performance of both tasks T_x and T_y in Fig. 3 for the two lengths of fiber recovered: 25 km (a) and 50 km (b). On this figure, the injection ratio P_{inj_y}/P_{inj_x} is fixed to 0.3. We can observe that there is an optimal injected power that yields the best mean performance at $P_{inj_x} = 0.09$ mW for 25 km and at $P_{inj_x} = 0.2$ mW for 50 km. We will only report this best value in the figures.

III. RESULTS

The results for the channel equalization of 25 km of propagation in the fiber are presented in Fig. 4(c). Figures 4(a) and 4(b) present an example of the signal at the input and output of the optical fiber, respectively. We observe that the performance on tasks T_x and T_y varies with the injection ratio P_{inj_y}/P_{inj_x} . If this ratio is smaller than 2, task T_x is better performed than task T_y . When this ratio is higher than 2, the trend is reversed, and the task T_y is better performed. This can be explained by a polarization switching in the VCSEL output induced by optical injection (i.e., the role of the dominant and depressed polarization modes of the VCSEL are exchanged²⁷). This phenomenon therefore increases the SNR of the task T_y injected in the depressed polarization mode. The system is able to provide a BER of 0.04% for the task T_x , while the dominant mode is strongly injected (with an injection ratio P_{inj_y}/P_{inj_x} of 0.2). The other task is processed with lower performance in this case, with a BER of 1.6%. When the ratio of power is greater than 0.5, the average performance of the reservoir reaches a threshold of performance with a BER of 0.35%. The ratio of injected power in the polarization modes can thereby be used to easily choose the split of performance between the two performed tasks. While processing a single nonlinear channel equalization task, the reservoir computer exhibits a BER of 0.08%.

To analyze the impact of the nonlinear transformation induced by our VCSEL-based reservoir on the task, we compare it to a

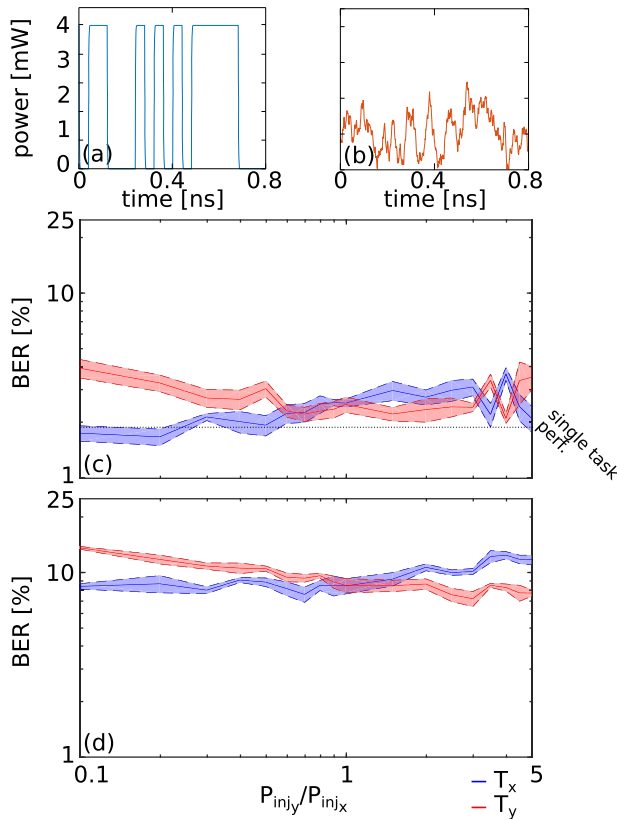


FIG. 5. Performance on the nonlinear channel equalization task after propagating 50 km in a communication channel made of optical fiber as a function of the ratio of injection P_{inj_y}/P_{inj_x} . (a) Example of the signal sent at the input of the fiber. (b) Corresponding received signal after 50 km of fiber. The blue curves corresponds to the performance of the task T_x , and the red curves corresponds to the performance of the task T_y for (c) the reservoir computer and (d) the linear classifier. The lighter area shows the standard deviation of the performance. The dotted line shows the performance of the reservoir performing the single task.

stand-alone linear regression (a *linear classifier*). Toward this end, the linear classifier is operated in the same conditions as the reservoir computer: One classifier is used to process the two tasks with the same dimension and similar injection power ratio as in a photonic reservoir computer. We use also the same input features with identical sizes for the training and testing sets (20 000 samples for training and 5380 for testing). Finally, similar SNR conditions are considered. To meet this last condition, as the VCSEL introduces additional noise, we added white noise to the input signal to achieve 21 dB before performing a stand-alone linear regression. With these similar operating conditions, a stand-alone linear regression provides a BER slightly lower than 1%, and the mean BER of the two tasks is $\sim 3.2\%$ in the best operating point identified in our experiment (i.e., for a ratio in the range of 0.6–3). The reservoir computer is thus able to improve the performance on the two tasks by approximately one order of magnitude.

We also provide results on the dual channel equalization of the propagation in 50 km of single mode fiber. Since the distortion of the signal is more pronounced [Fig. 5(b)], the mean performance of the reservoir computer is expected to be lower than the one after a 25 km transmission. The performance of the reservoir computer is given in Fig. 5(c).

We still observe a similar trend: The polarization switching of the VCSEL for a ratio of injection $P_{inj,y}/P_{inj,x} \sim 1$, and the best achieved BER for one task is at 1.6%. The best mean performance is at 2.2%, achieved for a ratio of injection at 0.7. The system performing this single task exhibits a BER of 1.9%, which is slightly below the performance previously reported.¹⁶ Contrary to the equalization of the shorter optical fiber, processing two tasks simultaneously slightly decreases the mean performance of the system, when compared to processing a single task.

The performance of the stand-alone linear regression (linear classifier) is presented in Fig. 5(d). The test has been realized with the same condition as the one used for the reservoir computer. The linear classifier is achieving a BER of 7.5% as a best performance. When both processed signals are balanced, the linear classifier exhibits its best mean performance, with a mean BER at 8.4%. Using the non-linear effects in our VCSEL-based photonic reservoir computer in similar SNR conditions thus provides a significant benefit, allowing to improve by a factor 5 the performance on the signal-recovery task.

The relatively low range of power used for the input signal propagating in the fiber is consistent with the range of power use in telecommunication networks. Furthermore, it does not lead to significant trigger of the Kerr nonlinearity. Equalizing both linear distortion and a strong Kerr effect remains a challenge in current digital signal processing (DSP)-based techniques for optical channel equalization.²⁸ To analyze how the Kerr effect would affect the performance of the reservoir, we have sent in the fiber two signals with a large pulse-amplitude modulation depth of 0.5 W and recover two signals simultaneously at the output of the fiber. This power is large enough to trigger the Kerr nonlinearity (as only a few tens of mW are necessary) and make the task more complex to solve. Under these new conditions and using similar parametric and operating conditions, our reservoir can now recover two signals simultaneously with an optimal mean BER of 8.9% for a 25 km fiber distortion and with a mean BER of 17.9% for a 50 km distortion. A degradation of at least one order of magnitude is observed in these conditions with the level of recovery unsuitable for telecom application. However, the level of

power was quite large, and no specific optimization was performed to optimize this modified task: There may be a more efficient size of the training set, larger reservoir size, and adapted preprocessing with more peripheral bits data to achieve better level of the performance. This work is left for future studies.

IV. CONCLUSION

We have realized an experimental photonic reservoir computer architecture capable of processing two tasks simultaneously. This reservoir is a time-delay reservoir computer, using a VCSEL as a physical node. The two different inputs are made by injecting two different optical signals, each being aligned with a different polarization mode of the VCSEL. Using this system, we have performed as an illustration two signal-recovery tasks simultaneously when the signal generated at 25 Gb/s is distorted by propagation in a 25 km or 50 km long SMF-28 optical fiber. We have been able to recover two signals with a BER of 0.3% at a processing speed of 51.3 Mb/s in total for a 25 km-distortion and with a BER of 3% at the same bit rate for a 50 km-distortion. On both tasks, the reservoir allows improving the performance by a factor 5–10, compared to processing the input signal directly under similar SNR conditions. The actual telecommunication networks use digital signal processing (DSP) to mitigate the effects of the optical fiber²⁹ as it allows propagating the signals along several thousands of kilometers with a BER of $\sim 10^{-3}$ compatible with forward error correction, but at the expense of important computational resources.

Our result also shows that there is still a significant margin of improvement before considering it a viable alternative to the best DSP approaches, despite achieving level of performance comparable to existing photonic-based machine learning techniques on this particular task.³⁰ Nevertheless, this result is a first step showing that analog photonic reservoir computing could be envisioned for such dual-tasking on optical channel equalization.

We proved in our previous work that the bimodal dynamics of the VCSEL allows better computational performance than a single mode dynamics system. This is due to a more complex dynamics that is suitable to perform computation. Here, we proved experimentally that we can exploit the bimodal dynamics of the VCSEL to process two tasks simultaneously. This suggests that using a system exhibiting more dynamical modes would allow scaling up the number of tasks to be processed simultaneously. However, performing several tasks simultaneously slightly degrades the mean computational performance of the system. There is thus a trade-off between the number of tasks to be processed and the individual performance of each task considered. Moreover, we hypothesize that the physics underlying the coupling mechanism between modes may also influence the performance of the reservoir computer, for instance, using longitudinal mode of a laser¹⁷ or the two modes of a semiconductor ring laser¹⁵ instead of using the polarization modes of the VCSEL. This may constitute an interesting frame for future studies of multimode reservoir computing.

ACKNOWLEDGMENTS

The authors acknowledge Chaire Photonique: Ministère de l'Enseignement Supérieur, de la Recherche et de l'Innovation;

Région Grand-Est; Département Moselle; European Regional Development Fund (ERDF); Metz Métropole; Airbus GDI Simulation; CentraleSupélec; and Fondation CentraleSupélec.

DATA AVAILABILITY

The data that support the findings of this study are available from the corresponding author upon reasonable request.

REFERENCES

- ¹H. Jaeger and H. Haas, "Harnessing nonlinearity: Predicting chaotic systems and saving energy in wireless communication," *Science* **304**, 78–80 (2004).
- ²W. Maass, T. Natschläger, and H. Markram, "Real-time computing without stable states: A new framework for neural computation based on perturbations," *Neural Comput.* **14**, 2531–2560 (2002).
- ³K. Vandoorne, P. Mechet, T. Van Vaerenbergh, M. Fiers, G. Morthier, D. Verstraeten, B. Schrauwen, J. Dambre, and P. Bienstman, "Experimental demonstration of reservoir computing on a silicon photonics chip," *Nat. Commun.* **5**, 3541 (2014).
- ⁴L. Larger, A. Baylón-Fuentes, R. Martinenghi, V. S. Udaltsov, Y. K. Chembo, and M. Jacquot, "High-speed photonic reservoir computing using a time-delay-based architecture: Million words per second classification," *Phys. Rev. X* **7**, 011015 (2017).
- ⁵J. Bueno, S. Maktoobi, L. Froehly, I. Fischer, M. Jacquot, L. Larger, and D. Brunner, "Reinforcement learning in a large-scale photonic recurrent neural network," *Optica* **5**, 756 (2018).
- ⁶F. D.-L. Coarer, M. Sciamanna, A. Katumba, M. Freiburger, J. Dambre, P. Bienstman, and D. Rontani, "All-optical reservoir computing on a photonic chip using silicon-based ring resonators," *IEEE J. Sel. Top. Quantum Electron.* **24**, 1–8 (2018).
- ⁷P. Antonik, N. Marsal, and D. Rontani, "Large-scale spatiotemporal photonic reservoir computer for image classification," *IEEE J. Sel. Top. Quantum Electron.* **26**, 1–12 (2020).
- ⁸L. Appeltant, M. C. Soriano, G. Van Der Sande, J. Danckaert, S. Massar, J. Dambre, B. Schrauwen, C. R. Mirasso, and I. Fischer, "Information processing using a single dynamical node as complex system," *Nat. Commun.* **2**, 466–468 (2011).
- ⁹Y. Paquot, F. Duport, A. Smerieri, J. Dambre, B. Schrauwen, M. Haelterman, and S. Massar, "Optoelectronic reservoir computing," *Sci. Rep.* **2**, 287 (2012).
- ¹⁰P. Antonik, M. Haelterman, and S. Massar, "Online training for high-performance analogue readout layers in photonic reservoir computers," *Cognit. Comput.* **9**, 297–306 (2017).
- ¹¹K. Takano, C. Sugano, M. Inubushi, K. Yoshimura, S. Sunada, K. Kanno, and A. Uchida, "Compact reservoir computing with a photonic integrated circuit," *Opt. Express* **26**, 29424–29439 (2018).
- ¹²F. Duport, B. Schneider, A. Smerieri, M. Haelterman, and S. Massar, "All-optical reservoir computing," *Opt. Express* **20**, 22783 (2012).
- ¹³D. Brunner, M. C. Soriano, C. R. Mirasso, and I. Fischer, "Parallel photonic information processing at gigabyte per second data rates using transient states," *Nat. Commun.* **4**, 1364–1367 (2013).
- ¹⁴K. Hicke, M. A. Escalona-Moran, D. Brunner, M. C. Soriano, I. Fischer, and C. R. Mirasso, "Information processing using transient dynamics of semiconductor lasers subject to delayed feedback," *IEEE J. Sel. Top. Quantum Electron.* **19**, 1501610 (2013).
- ¹⁵R. M. Nguimdo, G. Verschaffelt, J. Danckaert, and G. Van Der Sande, "Simultaneous computation of two independent tasks using reservoir computing based on a single photonic nonlinear node with optical feedback," *IEEE Trans. Neural Networks Learn. Syst.* **26**, 3301–3307 (2015).
- ¹⁶A. Argyris, J. Bueno, and I. Fischer, "Photonic machine learning implementation for signal recovery in optical communications," *Sci. Rep.* **8**, 8487 (2017).
- ¹⁷K. Harkhoe and G. V. D. Sande, "Delay-based reservoir computing using multimode semiconductor lasers: Exploiting the rich carrier dynamics," *IEEE J. Sel. Top. Quantum Electron.* **25**, 1 (2019).
- ¹⁸M. Müller, W. Hofmann, T. Gründl, M. Horn, P. Wolf, R. D. Nagel, E. Rönneberg, G. Böhm, D. Bimberg, and M. C. Amann, "1550-nm high-speed short-cavity VCSELs," *IEEE J. Sel. Top. Quantum Electron.* **17**, 1158–1166 (2011).
- ¹⁹J. Vatin, D. Rontani, and M. Sciamanna, "Enhanced performance of a reservoir computer using polarization dynamics in VCSELs," *Opt. Lett.* **43**, 4497 (2018).
- ²⁰J. Vatin, D. Rontani, and M. Sciamanna, "Experimental reservoir computing using VCSEL polarization dynamics," *Opt. Express* **27**, 18579 (2019).
- ²¹X. Guo, S. Xiang, Y. Zhang, L. Lin, A. Wen, and Y. Hao, "Polarization multiplexing reservoir computing based on a VCSEL with polarized optical feedback," *IEEE J. Sel. Top. Quantum Electron.* **26**, 1 (2019).
- ²²R.-J. Essiambre, G. Kramer, P. J. Winzer, G. J. Foschini, and B. Goebel, "Capacity limits of optical fiber networks," *J. Lightwave Technol.* **28**, 662–701 (2010).
- ²³R. Lang and K. Kobayashi, "External optical feedback effects on semiconductor injection laser properties," *IEEE J. Quantum Electron.* **16**, 347–355 (1980).
- ²⁴G. P. Agrawal, "Nonlinear fiber optics," in *Nonlinear Science at the Dawn of the 21st Century*, edited by P. L. Christiansen, M. P. Sørensen and A. C. Scott (Springer Berlin Heidelberg, Berlin, Heidelberg, 2000), pp. 195–211.
- ²⁵K. Hammani, B. Kibler, C. Finot, P. Morin, J. Fatome, J. M. Dudley, and G. Millot, "Peregrine soliton generation and breakup in standard telecommunications fiber," *Opt. Lett.* **36**, 112 (2011).
- ²⁶A. Argyris, J. Bueno, and I. Fischer, "PAM-4 transmission at 1550 nm using photonic reservoir computing post-processing," *IEEE Access* **7**, 37017–37025 (2019).
- ²⁷M. Sciamanna, K. Panajotov, H. Thienpont, I. Veretennicoff, P. Mégret, and M. Blondel, "Optical feedback induces polarization mode hopping in vertical-cavity surface-emitting lasers," *Opt. Lett.* **28**, 1543–1545 (2003).
- ²⁸P. J. Winzer, D. T. Neilson, and A. R. Chraplyvy, "Fiber-optic transmission and networking: The previous 20 and the next 20 years [invited]," *Opt. Express* **26**, 24190 (2018).
- ²⁹N. Eiselt, J. Wei, H. Griesser, A. Dochhan, M. H. Eiselt, J.-P. Elbers, J. J. Vegas Olmos, and I. T. Monroy, "Evaluation of real-time 8 × 56.25 Gb/s (400 G) PAM-4 for inter-data center application over 80 km of SSMF at 1550 nm," *J. Lightwave Technol.* **35**, 955–962 (2017).
- ³⁰D. Zibar, M. Piels, R. Jones, and C. G. Schäffer, "Machine learning techniques in optical communication," *J. Lightwave Technol.* **34**, 1442–1452 (2016).